Journal of Sol-Gel Science and Technology (2018) 87:137–146
https://doi.org/10.1007/s10971-018-4698-7

ORIGINAL PAPER: NANO-STRUCTURED MATERIALS (PARTICLES, FIBERS, COLLOIDS, COMPOSITES, ETC.)

Synthesis, characterization, multifunctional electrochemical (OGR/ORR/SCs) and photodegradable activities of $ZnWO_4$ nanobricks

Saad M. Alshehri[1] · Jahangeer Ahmed[1] · Tansir Ahamad[1] · Norah Alhokbany[1] · Prabhakarn Arunachalam[1] · Abdullah M. Al-Mayouf[1] · Tokeer Ahmad[2]

Received: 4 April 2018 / Accepted: 17 May 2018 / Published online: 5 June 2018

Abstract

Brick-shaped zinc tungstate nanoparticles have been synthesized by ecofriendly solvent-free process using molten salts. Zinc tungstate nanobricks ($ZnWO_4$ Nbs) were characterized by powder x-ray diffraction (PXRD), FTIR, Raman, energy dispersive and electron microscopic studies. $ZnWO_4$ Nbs are used as the multifunctional electrode materials to oxygen generation reactions (OGR), oxygen reduction reactions (ORR) and supercapacitors (SCs) as well as photo-catalysts in the waste-water treatment by the degradation of organic dyes. Low overpotential ($\eta_{10} = 0.475$ V), low tafel slope (140 mV/dec), high current density (~70 mA/cm^2) and good stability of the electrodes are the key results of the present studies for water electrolysis (OGR/ORR). $ZnWO_4$ Nbs have also shown great interest in supercapacitors with efficient charge–discharge activities in 1 M KOH. The specific capacitance and energy density of $ZnWO_4$ Nbs were found to be 250 F/g and 80 Wh/kg, respectively, at 5 mV/s, these values are relatively higher than that of previously reported specific capacitance and energy density value of metal tungstate nanoparticles. $ZnWO_4$ Nbs as the photo-catalysts work very significantly for photocatalytic degradation of aqueous MB dye solution (~85 % in 3 h) in neutral medium.

Graphical Abstract

$ZnWO_4$ Nanobricks show significant multifunctional electro-chemical activities in alkaline medium and photocatalytic degradation of organic dye in neutral medium.

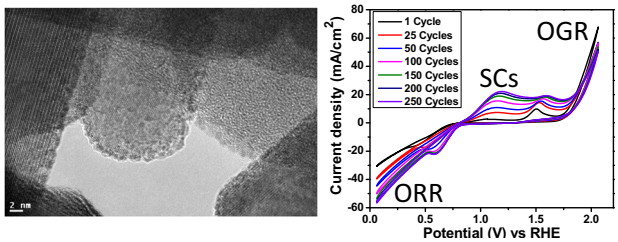

✉ Saad M. Alshehri
alshehri@ksu.edu.sa

✉ Jahangeer Ahmed
jahmed@ksu.edu.sa

[1] Department of Chemistry, College of Science, King Saud University, Riyadh 11451, Saudi Arabia

[2] Nanochemistry Laboratory, Department of Chemistry, Jamia Millia Islamia, New Delhi 110025, India

Highlights

- Ecofriendly solvent-free Synthesis of $ZnWO_4$ Nanobricks (Nbs).
- $ZnWO_4$ Nbs show admirable multifunctional electrochemical activities (OGR/ORR/SCs).
- Low overpotential, low Tafel values, relatively high current density and good stability of electrode materials are significant for OGR and ORR.
- $ZnWO_4$ Nbs exhibit efficient supercapacitor performances with the specific capacitance (250 F/g) and energy density (80 Wh/kg) at 5 mV/s in 1 M KOH.
- $ZnWO_4$ Nbs also work as photo-catalysts to enhance the degradation of aqueous organic dyes.

Keywords Zinc tungstate · Nanoparticles · Electrocatalysis · Oxygen reduction · Photocatalysis

1 Introduction

Environmental remediation and clean energy production have been attracted to the scholars, worldwide, since last two decades. Precious electrode materials (e.g. Pt, Ru, Ir etc. or their oxides) are commonly used globally in the development of energy conversion process [1–4]. Replacement of these precious electrode materials by cost effective, eco-friendly and promising nature of the electrodes is the current challenge to develop the new technologies for clean, renewable and sustainable energy resources. However, present work focuses on the enhanced electrochemical performances of multi-functional $ZnWO_4$ Nbs electrodes in water electrolysis (OGR and ORR) and supercapacitor applications. The demand of renewable energy and the diminution of fossil fuels have been increased drastically, while the contaminated water causes harmful effects on human being [5, 6]. Therefore, production of cleaned renewable energy and controlling of environmental pollutions are the current challenges. The removal of organic dyes (cationic/ anionic/ neutral) from waste-water via photocatalytic oxidation reaction is an efficient and cost-effective way to control the environmental problems [7]. Nanocrystalline $ZnWO_4$ particles have also been reported as the efficient photo-catalysts in the degradation of organic dyes [8–13].

$ZnWO_4$ nanostructures were also reported as supercapacitors [14–16], sensors [17–19], and photo-electrocatalysts [20, 21]. $ZnWO_4$ as a pure electro-catalyst is still traceless in the electrolysis of water to gas evolution and reduction reactions. Other materials like transition metal tungstate nanoparticles were also reported as electrocatalysts in water electrolytic reaction and supercapacitors [22–25]. Low overpotential, low Tafel values and stability of the electrodes are the significant features to improve the electrochemical activities of the electrode materials. The overpotentials of metal tungstate nanoparticles are reported from 380 – 970 mV for water splitting [22–24]. High over-potential range could be accountable to diminish the electrochemical performances. On the other hand, graphene based electrode materials have been used extensively for the supercapacitor applications due their chemical stability, high surface area and pore volume, good conductivity and capacitive performances. The specific capacitances of graphene oxide and graphene- metal oxide nanocomposites were reported in the range from 40 to 213 F/g [26, 27]. Zinc, nickel and copper tungstate nanostructured materials have shown the specific capacitance values of ~40–72 F/g (3 M KOH) [14], ~171 F/g (2 M KOH) [28] and ~13 F/g (2 M KOH) [29], respectively. Recently, we have devolved various nano-structured materials with controlled morphology for photocatalytic degradation of organic pollutants, electrochemical water splitting and supercapacitors [30–34]. Synthesis of single phase materials is also an important concern. $ZnWO_4$ nanostructured materials were synthesized from the various routes including hydrothermal [35–37], polyol [38], mechanochemical [39], microwave [40, 41], microwave-solvothermal [42], and ultrasonic spray pyrolysis [43]. Previously, molten salts flux method was employed in the synthesis of $ZnWO_4$:Eu^{3+} nanoparticle (particle size ~50 nm) using variety of flux i.e. $LiNO_3$, $NaNO_3$ and KNO_3 [44].

In this paper, we report the solvent-free synthesis of $ZnWO_4$ nanoparticles with unusual morphology using molten salts ($NaNO_3 + KNO_3$). Note that the solvent-free process is an ecofriendly approach to prepare the nanostructured materials for various applications. $ZnWO_4$ Nbs were successfully characterized by PXRD, FTIR, Raman, FESEM, HRTEM and energy dispersive studies. Water electrolysis of $ZnWO_4$ Nbs was investigated in details at room temperature on 3–electrode electrochemical work station (3-EEWS) using cyclic voltammetry (CV), linear sweep voltammetry (LSV) with rotating disk electrode (RDE) and Tafel experiments. CV and charge–discharge measurements were carried out to study the supercapacitor application of the $ZnWO_4$ Nbs electrode materials. Enhanced photocatalytic activities of $ZnWO_4$ Nbs were also examined for the degradation of hazardous organic dyes in to non-hazardous substances under sun light irradiations in neutral medium.

2 Experimental

Solvent-free process consists of 2 moles of zinc nitrate hexahydrate ($Zn(NO_3)_2.6H_2O$, BDH, 98%), 2 mole of sodium tungstate dehydrate ($Na_2WO_4.2H_2O$, BDH, 96%), 60 moles of sodium nitrate ($NaNO_3$, Alfa Aesar, 98 + %) and 60 moles of potassium nitrate (KNO_3, Alfa Aesar, 99%). The above mixture was ground together properly to make a homogenous reacting mixture followed by the firing at 500 °C for 6 h. The reaction conditions have been fixed on the basis of phase diagram of the molten salts [$NaNO_3$ and KNO_3] as also reported elsewhere [45]. The resulting products were washed by de-ionized water several times and then dried in oven at 60 °C. The final product was white in color. The white-colored product was characterized by PXRD to confirm the percent phase purity and crystal structure of $ZnWO_4$ Nbs. PXRD data of $ZnWO_4$ Nbs was collected on powder x-ray diffractometer (Rigaku MiniFlex,

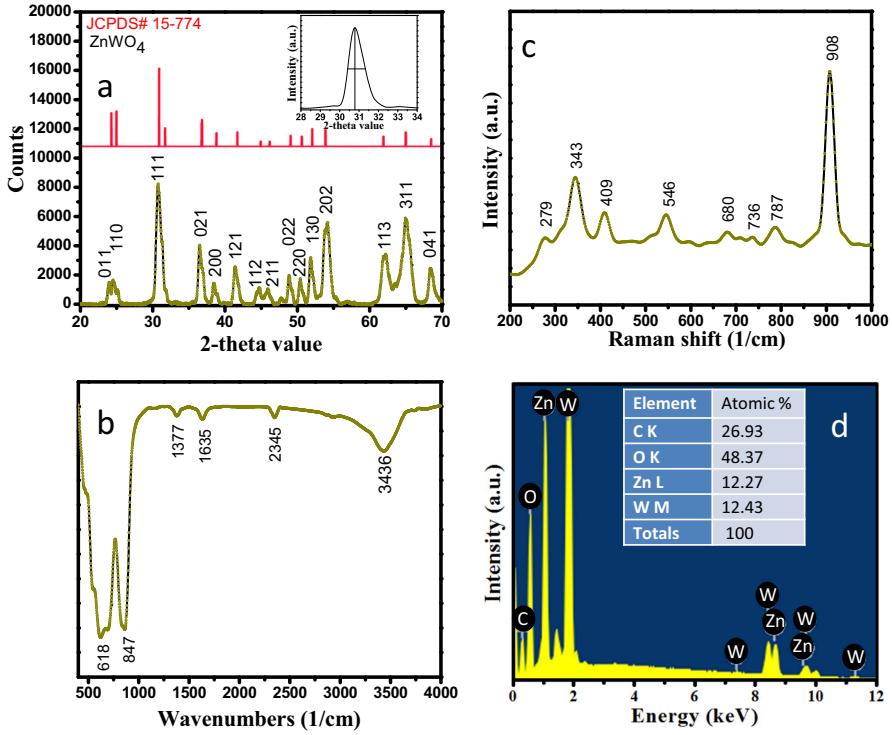

Fig. 1 (**a**) PXRD, (**b**) FTIR, (**c**) Raman, and (**d**) EDS studies of $ZnWO_4$ Nbs. Inset of (**a**) shows FWHM of X-ray line broadening studies of $ZnWO_4$ Nbs

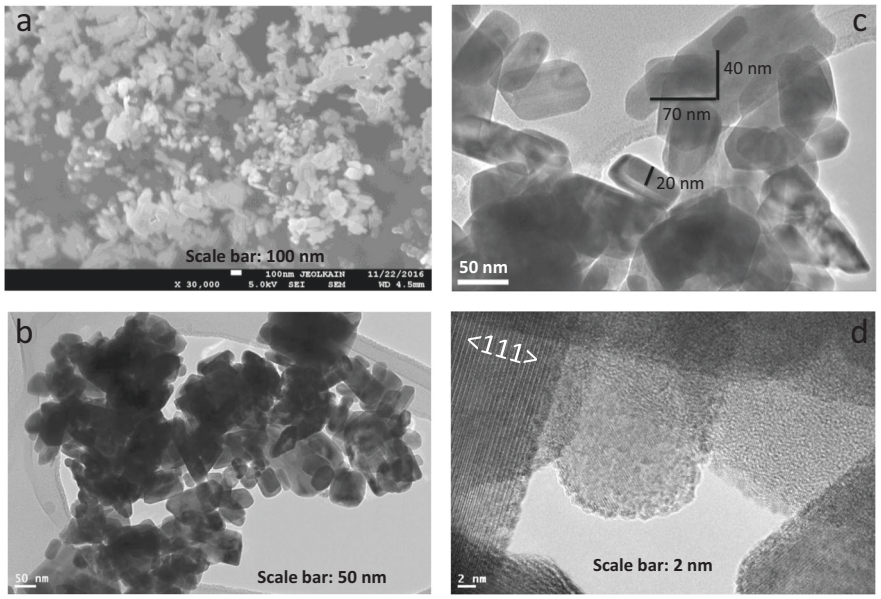

Fig. 2 (**a**) FESEM, (**b**, **c**) TEM, (**d**) HRTEM images of $ZnWO_4$ Nbs

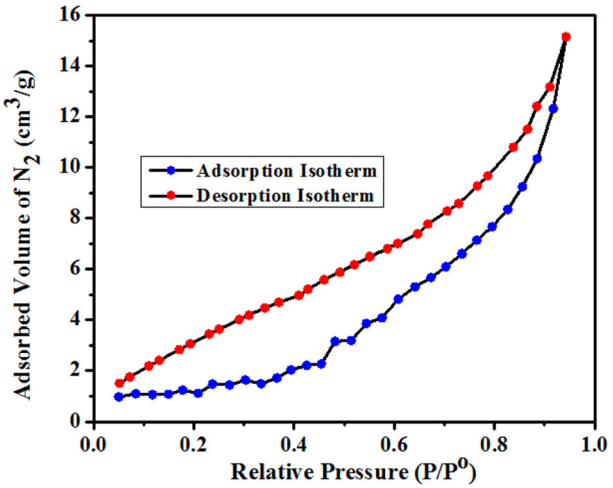

Fig. 3 N_2—adsorption–desorption isotherm of $ZnWO_4$ Nbs

Ni-filtered Cu-Kα radiation, step size of 0.02° and scan speed of 1 s). FTIR spectrum of $ZnWO_4$ Nbs was recorded in the range of wavenumber (per cm) from 400 to 4000 per cm on a Bruker TENSOR 27 Spectrometer. Field emission scanning electron microscope (FESEM) and EDS studies of $ZnWO_4$ Nbs were investigated at 5KV (JEOL, JSM-7600F), while HR-TEM data were collected at 200 kV (JEOL, JSM-2100F). The surface area of $ZnWO_4$ Nbs was measured by the Brunauere–Emmett–Teller (BET) measurements (V-Sorb 2800 Porosimetry Analyser, Gold APP Instruments). Electrochemical activities and stability of the electro-catalysts were tested by Cyclic voltammetry (CV), linear sweep voltammetry (LSV), charonoamperometry (CA), RDE measurements on potentiostat–galvanostat (CHI 660E, China) electrochemical analyzer at 25 °C. Three electrodes [i.e. reversible hydrogen electrode (RHE) as reference, Pt wire as counter and glassy carbon electrode or carbon sheet as working electrode] were used in the electrochemical studies of $ZnWO_4$ Nbs. The working electrode for water electrolysis has been prepared by pasting the slurry on the glassy carbon (GC) electrode. The slurry contains 2.5 mg of $ZnWO_4$ catalysts, 0.5 ml of isopropanol and 0.1 ml of nafion solution. The prepared working electrode was dried in oven at 50 °C prior to use in electrolysis of water. Loaded amount of $ZnWO_4$ catalysts on GC electrode was of 0.28 mg/cm^2. The area of GC working electrode was 0.07 cm^2. Electrolysis of water (OER and ORR) was carried in 1.0 M KOH at 25 °C vs. reversible hydrogen electrode (RHE). ORR reaction was also performed using rotating disc electrode during LSV at the rotations of 500 to 3000 r.p.m. Moreover, we have studied the supercapacitive behavior of $ZnWO_4$ Nbs using 1.0 M KOH electrolyte. The scan rates vary from 5 to 200 mV/s during the CV measurements of $ZnWO_4$ Nbs. The specific capacitance and energy density of the electrodes were estimated using the respective

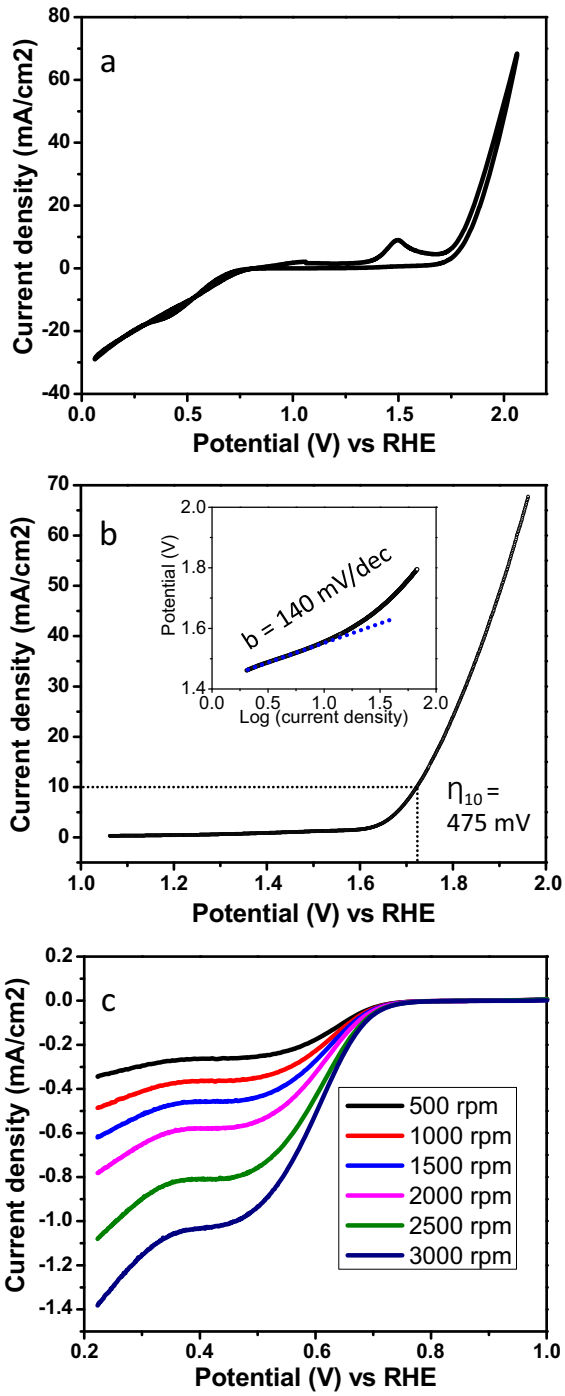

Fig. 4 (**a**) CV of $ZnWO_4$ Nbs for OGR and ORR, (**b**) LSV of $ZnWO_4$ Nbs for OGR, (**c**) LSV of $ZnWO_4$ Nbs for ORR at different rotations (500–3000 r.p.m.). Inset of (**b**) representing Tafel plot of $ZnWO_4$ Nbs

equations as also given in results and discussion. Zinc tungstate electrodes for supercapacitor were prepared by electrophoretic deposition on carbon sheet. Typically, 3 mg of iodine (Alfa Aesar) and 15 mg of zinc tungstate powder were dispersed in 15 ml of acetone followed by sonication in ultrasonic water bath for 15 mins to obtain uniform

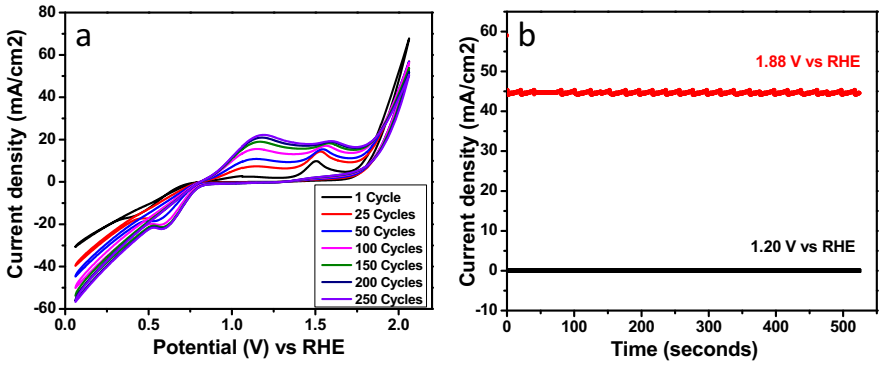

Fig. 5 (**a**) Cyclic voltammograms and (**b**) chronoamerometric studies of $ZnWO_4$ Nbs electrode for stability

dispersed zinc tungstate nanopowders. The carbon paper was immersed, parallel to each other, in the solution with ca. 1.0 cm of distance, and then + 10 V of bias was applied between them for 4 min using a potentiostat (BioLogic SAS, model). Thereafter, the electrodes were rinsed with de-ionized water, dried in air and then calcined at 80 °C for 120 min under air atmosphere. The average weight of zinc tungstate deposited on carbon paper was 2.2 mg. The photocatalytic performances of $ZnWO_4$ Nbs were investigated on UV-VISIBLE spectrophotometer (SHIMADZU, UV-1650) for photodegradation of MB dye in neutral medium (pH = 7) at λ_{max} of 664 nm under the solar light irradiation.

3 Results and discussion

The crystal structure and the phase purity of freshly prepared materials were tested by PXRD. Figure 1a shows the PXRD patterns of $ZnWO_4$ that can be indexed with monoclinic structure of $ZnWO_4$. PXRD patterns show the formation of high crystalline materials with zero impurity phases of other oxides (i.e., ZnO, WO_3) or molten salts. The indexed JCPDS pattern number of $ZnWO_4$ is 15–774. Inset of Fig. 1a shows x-ray line broadening studies of $ZnWO_4$. The X-ray line broadening studies have been used to determine the crystallite size of $ZnWO_4$ using Scherrer's Formula [$t = 0.9\lambda / (B\cos\theta)$]; where t, λ and B are the diameter of particle, wavelength of CuKα radiation and line broadening, respectively. B can be calculated by Warren's formula (i.e., $B^2 = B^2_M - B^2_S$), where B_M and B_S are full width half maxima (FWHM) of powder sample and standard (i.e. quartz) respectively. The crystallite size of $ZnWO_4$ Nbs was found to be ~ 45 (± 5) nm from line broadening studies. Figure 1b represents the FT-IR spectrum of $ZnWO_4$. The characteristics IR bands at ~618 and ~847 per cm can be ascribed to ν(Zn–O–Zn) and ν(W–O), respectively. The strong and weak bands at ~3436 and ~1635 per cm are indexed with – OH group that could be due to the presence of atmospheric moisture. IR bands at ~2360 and ~1384 per cm resemble to C = O and C–O groups, respectively, of atmospheric CO_2. Raman spectrum of $ZnWO_4$ Nbs is shown in Fig. 1c. The characteristic Raman bands are identified at 279 (A_g), 311 (A_g), 343 (A_g), 409 (A_g), 510 (B_g), 546 (A_g), 680 (B_g), 736 (A_g), 787 (B_g), and 908 (A_g) cm^{-1} arise from $ZnWO_4$ Nbs as also reported [46]. These phonon bands confirm the formation of wolframite-type structure of $ZnWO_4$ Nbs. Figure 1d shows the energy dispersive X-ray spectroscopic (EDS) studies to investigate the elemental composition of $ZnWO_4$. Note that EDS was equipped with FESEM machine operated at 5 kV. The elemental weight fraction (i.e., atomic weight) in the nanoparticles was found to be in the ratio of 1:1:4 of Zn:W:O, respectively, as it was expected according to our preliminary loaded composition.

FESEM and HRTEM studies were carried out for the morphology and the particle size of $ZnWO_4$ nanostructured materials (Fig. 2). FESEM image shows that the particles of $ZnWO_4$ materials are in nanometric region with an unusual morphology (Fig. 2a). TEM and HRTEM micrographs confirm the formation of nano-sized particles of $ZnWO_4$ in bricks shape (Fig. 2b, c). The length, width, and height of the $ZnWO_4$ Nbs were observed to be 70, 40, and 20 nm, respectively. Figure 2d shows the HRTEM micrograph of $ZnWO_4$ Nbs to observe the crystalline nature and the interplanar distance (i.e., *d*-spacing). The d-spacing value of $ZnWO_4$ Nbs was calculated using the HRTEM data, which matches with the most intense line of PXRD patterns of monoclinic crystal structure of $ZnWO_4$ Nbs. The surface area of $ZnWO_4$ Nbs has been studied with the help of BET isotherm i.e., N_2 adsorption–desorption isotherm as shown in Fig. 3. The BET surface area, pore volume, and pore radius of $ZnWO_4$ Nbs were found ~13.40 m^2/g, 0.028 cc/g and 18.78 Å, respectively. The resulting surface area of $ZnWO_4$ Nbs is nearly similar to previously reported surface area of zinc tungstate nanoparticles [9, 39].

Electro-chemical studies of $ZnWO_4$ Nbs for water electrolysis (OGR and ORR) and supercapacitor were investigated in 1.0 M KOH. Anodic and cathodic sweeps were observed in cyclic voltammetry (CV) with a very sharp redox peak of ~1.49 V vs. RHE at the scan rate of 50 mV/s

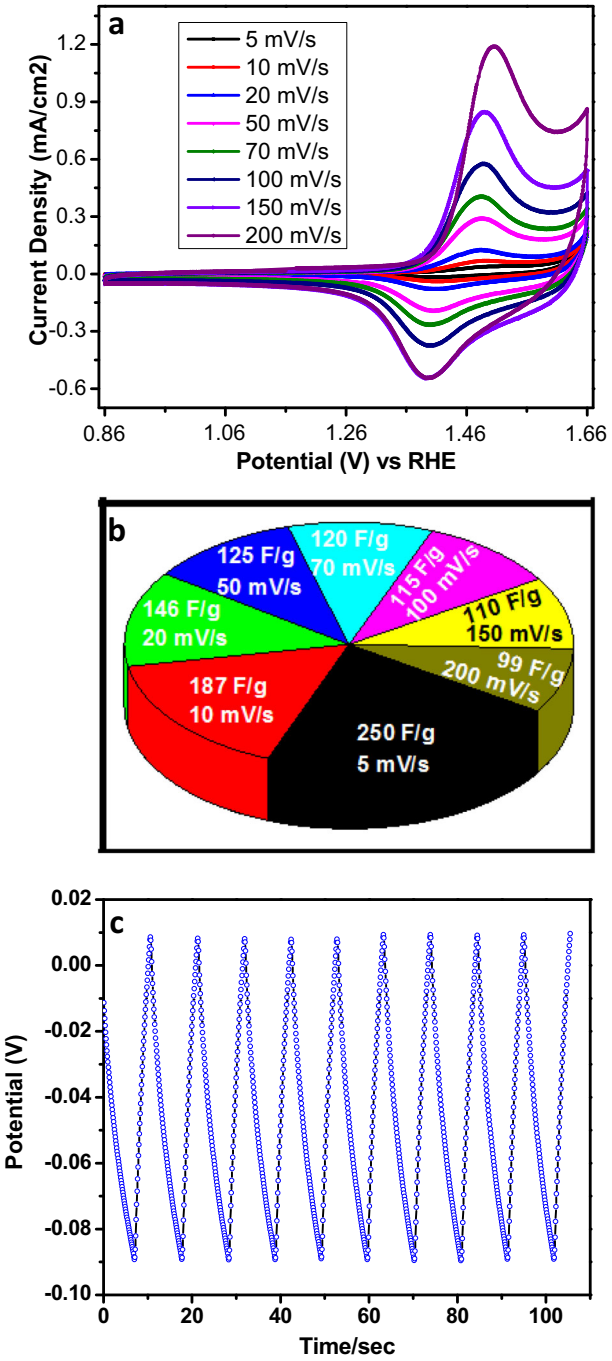

Fig. 6 (**a**) CV curves and (**b**) histogram showing the resulting specific capacitance of $ZnWO_4$ Nbs electrode at different scan rate from 5 to 200 mV/s. (**c**) Charge–discharge (CD) curves of $ZnWO_4$ Nbs for IR drops within 20 segments

(Fig. 4a). This initial study shows the multi-functional behavior of the electro-catalysts in alkaline medium. Thereafter, LSV polarization studies were carried out for OGR and ORR. Figure 4b shows the polarization curve of $ZnWO_4$ Nbs for the OGR in 1.0 M KOH vs. RHE at the scan rate of 50 mV/s. The current density was found to be ~70 mA/cm^2. The resulting current density of $ZnWO_4$ Nbs for OGR is the function of surface area of the nanoparticles used and a combination of both faradaic and non-faradaic processes. The current density is directly related to the amount of oxygen generate during the water oxidation reaction. The overpotanetial was found to be 475 mV at the current density of 10 mA/cm^2 (η_{10}) by the exclusion of the potential of water oxidation process. Inset of Fig. 4b shows the Tafel plot of the potential (η, V) vs. log (current density), which is used to study the energy consumption in water oxidation reaction for OGR ($2H_2O_{(l)} \rightarrow 4H^+ + 4e^-{}_+ O_{2(g)}$). Tafel plot is linearly fitted and the slope value of $ZnWO_4$ Nbs was found to be ~135 mV/dec. Present Tafel slop value for water oxidation reaction is relatively lower than the previous reports. An effective catalyst for water oxidation could have low over-potential and low Tafel values to sustain high current with stability of the electrodes to enhance the production of energy, due to low consumption of energy in electrochemical reactions. Figure 4c shows the polarization curves for ORR using the rotating disk electrode (RDE) by applying cathodic potential vs. RHE with scan rate of 10 mV/s. The rotations of RDE vary from 500 to 3000 r.p.m. for the ORR studies. This is noteworthy that the diffusion current densities of $ZnWO_4$ Nbs were significantly increased with the speed due to oxygen diffusion distance. Koutecky–Levich (K–L) equation [47, 48] was employed to understand the kinetics of water splitting and also used to study the electrons convoluted in the reduction reactions. The electro-chemical O_2 reduction reactions follow the 1st order kinetics and 4e$^-$ transferred process in electrolysis of water. The stability test of $ZnWO_4$ electro-catalysts was studied during the water redox reactions (OGR and ORR) for 250 cycles in 1.0 M KOH at 50 mV/s (Fig. 5a). The onset potentials and current densities of $ZnWO_4$ Nbs were consistent up to 250 cycles. Additionally, to confirm the stability of the electrode materials in water redox reactions, chrono-amerometric (CA) tests of $ZnWO_4$ Nbs were also carried out at 1.88 V vs. RHE for 525 s (Fig. 5b). CA is a potentio-static and true quantitative experiment. From the CA studies, we observed that the current density (~44 mA/cm^2) is stable with time at 1.88 V as also recorded the same during CV. Therefore, the present work confirms the long-term stability of $ZnWO_4$ Nbs as the bifunctional electro-active electrode materials in water electrolysis to OGR and ORR activities. Precious electro-active materials (e.g., Pt, Ru, Ir) were reported as the superior electro-catalysts in water splitting reactions. However, the materials with earth abundant elements are significant electro-catalysts in water splitting reactions and very economical compared to the noble materials.

Moreover, the electrochemical performances of $ZnWO_4$ Nbs were investigated for the supercapacitors. The capacitive performances of the prepared electrodes were investigated on the electrochemical work station using CV

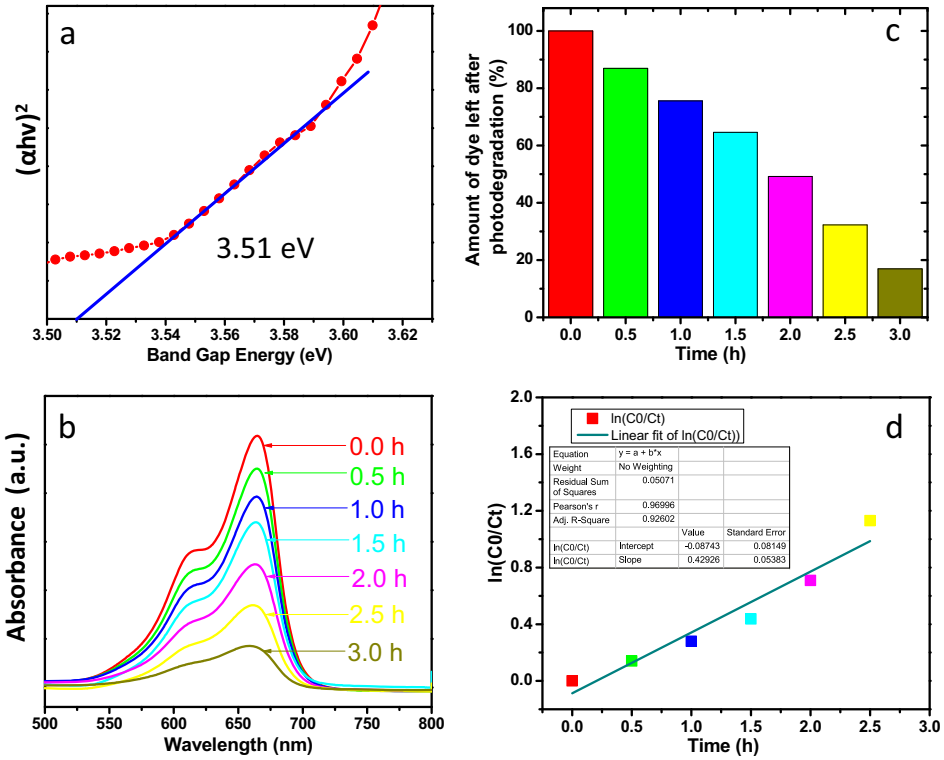

Fig. 7 (**a**) Band gap energy plot, (**b**) absorption spectra, (c) percent photo-degradation and (**d**) linear plots of photocatalytic degradation of MB dye with $ZnWO_4$ Nbs in neutral medium

measurements. The specific capacitance of the electrodes can be determined using the following equation: $Cs = [(\int I(V)dv) / (vm\Delta V)]$, where Cs, $\int I(V)dv$, v, m, and ΔV are the specific capacitance (F/g), integrated area under the CV curve, scan rate (mV/s), mass of the catalysts (g), and voltage window (V) respectively. Figure 6a shows the CV curves of $ZnWO_4$ Nbs electrodes at the various scan rates of 5, 10, 20, 50, 70, 100, 150 and 200 mV/s within the peak window of 0.86–1.66 V vs. RHE. CV curves show sharp anodic (~1.49 V) and cathodic (~1.40 V) peaks in the applied potential window. This could be due to the charge storage behavior of the materials by the faradaic electron charge-transfer process (i.e., faradaic redox reaction). $ZnWO_4$ electrode gives high integrated area which reveals high energy storage capacity of the materials. We observed that the peak current increases with the scan rates (5–200 mV/s), which is also a good agreement of the rate capability and capacitive behavior of the electrode materials. The specific capacitance of $ZnWO_4$ Nbs was determined to be ~250 F/g using CV at 5 mV/s. The performance of $ZnWO_4$ supercapacitor was found superior than reported $CuWO_4$ (10 F/g) and $ZnWO_4$ (70 F/g at 5 mV/s) supercapacitors [14, 29]. The maximum specific capacitance of 171 F/g was reported for $NiWO_4$ nanoparticles [28]. The specific capacitances of the electrode have been estimated at the various scan rates as also shown in Fig. 6b. The energy density (E) of $ZnWO_4$ Nbs was also determined using the following equation: $E = (Cs \times \Delta V^2) / 2$. The energy density of $ZnWO_4$ Nbs was found to be 80 Wh/kg at the scan rate of 5 mV/s. Carbon based electrode materials like carbon nanotubes (CNT), graphene (G), graphene oxide (GO) or their nanocomposites have been used extensively as the structural stabilizers, promoters, conductive additives, or reactive precursors to improve the power density and energy storage capacities of the electrodes [49–51]. The capacitive performances of graphene oxide (213 F/g) [26], graphene/ZnO (60–120 F/g) [26, 27], and graphene/SnO_2 (42 F/g) [27] were also found weaker than the present results. Open circuit potential charge–discharge (CD) curves (potential (V) vs. time) of $ZnWO_4$ Nbs were shown in Fig. 6c. The CD experiments were conducted at the current density of 0.1 A/g. CD curves of $ZnWO_4$ Nbs exhibit reversible cycles through charge and discharge route for 20 segments. Small IR drops were detected during discharge path. Low IR drops of $ZnWO_4$ Nbs are good indicators for low electrode/electrolyte interfacial resistance and low energy loss. The discharge time is also an important concern to study the super-capacitive behavior of the materials. The discharge time was found to be ~110 seconds only for 20 segments. High discharge time of $ZnWO_4$ Nbs is directly related to high Cs that is also a good agreement with the CV.

Additionally, photocatalytic properties of $ZnWO_4$ Nbs were investigated using the UV-visible absorption spectroscopy. The band gap of $ZnWO_4$ Nbs was found to be ~3.51 eV, which is calculated from the absorption data using Tauc's model [52]. Figure 7a shows a plot between

band gap energy and $(\alpha h\nu)^2$ of $ZnWO_4$ Nbs. Where ν, h and α symbolize frequency, Planck's constant and the absorbance of incident light beam respectively. The band gap of $ZnWO_4$ Nbs (~3.51 eV) was found to be lower than the reported value (~3.8 eV) [53]. The band gap is an energy difference of valance and conduction bands. Photo-catalytic behavior of $ZnWO_4$ Nbs was also investigated for the degradation methylene blue (MB) dye solution in presence of full sun light at neutral medium. Figure 7b shows the UV-visible absorption spectra of photodegradation of MB dye at the maxima of ~664 nm for 3 h. The absorption intensities of dye have been reduced consistently with time in under sun light irradiation. This result shows that $ZnWO_4$ Nbs work as admirable photo-catalysts in the degradation of organic pollutants like dyes. Photocatalytic degradation of MB dye can be explained by the formation of $OH^{\bullet}$ and $O_2^{-\bullet}$ (hydroxyl and super-oxide free radicals) from electron (e^-)-hole (h^+) pairs followed by the attack on the dye molecule to oxidize in inorganic minerals (i.e., NO_3^-, H_2O, NH_4^+, CO_2). The mechanism of photocatalytic degradation of dyes over the surface of photo-catalysts is reported elsewhere [30, 31, 53]. Figure 7c shows the percent photodegradation of dye with time. $ZnWO_4$ photo-catalysts degrade the dyes of ~85% in 3 h under the irradiation of full sun light, while neither degradation or adsorption of dye solution was occurred in dark with $ZnWO_4$. The photocatalytic activity of $ZnWO_4$ Nbs in neutral medium was found to be better than the previously reported photocatalysis of other metal tungsten oxides [54]. Recently, WO_3 nanoparticles were used as the photo-catalysts in the degradation of MB dye solution, which degrade the dye of ~25 % in ~3 h [55]. The linear plot (ln (C_0/C_t) vs. time) follows the pseudo-first order kinetics as shown in Fig. 7d. The rate constants (k) and R^2 were found to be ~0.43/min and ~0.93, respectively.

4 Conclusion

In summary, brick-shaped $ZnWO_4$ nanoparticles were successfully synthesized by the solvent-free process using molten salts. Efficient multifunctional electrochemical (OGR/ORR/SCs) and photo-catalytic properties of $ZnWO_4$ Nbs were investigated for cleaned renewable energy, storage and environmental remediation, respectively. $ZnWO_4$ Nbs show excellent electro-catalytic behavior in water electrolysis (i.e. OGR/ORR) with low overpotential, low tafel slope, high current density and good stability of electrode materials. $ZnWO_4$ Nbs also work as the promising supercapacitors. CV results show high specific capacitance and energy density of 250 F/g and 80 Wh/kg, respectively, at 5 mV/s in 1 M KOH. Enhanced photocatalytic performances of $ZnWO_4$ Nbs were also conducted for photodegradation of dyes at pH of 7. Therefore, the present work suggests that $ZnWO_4$ Nbs are potential materials and can be used traditionally as multifunctional catalytic materials in energy conversion, conservation, storage and environmental remediation.

Acknowledgements We extend our sincere appreciation to the Deanship of Scientific Research at King Saud University for funding this Research Group (RG-1435-007).

Compliance with ethical standards

Conflict of interest The authors declare that they have no conflict of interest.

References

1. Gutsche C, Moeller CJ, Knipper M, Borchert H, Parisi J, Plaggenborg T (2016) Synthesis, structure, and electrochemical stability of Ir-decorated RuO_2 nanoparticles and Pt nanorods as oxygen catalysts. J Phys Chem C 120(2):1137–1146. https://doi.org/10.1021/acs.jpcc.5b11437
2. Ahmed J, Mao Y (2016) Ultrafine iridium oxide nanorods synthesized by molten salt method toward electrocatalytic oxygen and hydrogen evolution reactions. Electrochim Acta 212:686–693. https://doi.org/10.1016/j.electacta.2016.06.122
3. Reier T, Oezaslan M, Strasser P (2012) Electrocatalytic oxygen evolution reaction (OER) on Ru, Ir, and Pt catalysts: a comparative study of nanoparticles and bulk materials. ACS Catal 2 (8):1765–1772. https://doi.org/10.1021/cs3003098
4. Audichon T, Napporn TW, Canaff C, Morais C, Comminges C, Kokoh KB (2016) IrO_2 coated on RuO_2 as efficient and stable electroactive nanocatalysts for electrochemical water splitting. J Phys Chem C 120(5):2562–2573. https://doi.org/10.1021/acs.jpcc.5b11868
5. Zhang Q, Huang Y, Peng S, Zhang Y, Shen Z, Cao JJ, Ho W, Lee SC, Pui DYH (2017) Perovskite $LaFeO_3$-$SrTiO_3$ composite for synergistically enhanced NO removal under visible light excitation. Appl Catal B Environ 204:346–357. https://doi.org/10.1016/j.apcatb.2016.11.052
6. Zhang Q, Huang Y, Xu L, Cao JJ, Ho W, Lee SC (2016) Visible-light-active plasmonic Ag-SrTiO3 nanocomposites for the degradation of NO in air with high selectivity. ACS Appl Mater Interfaces 8(6):4165–4174. https://doi.org/10.1021/acsami.5b11887
7. Guo S, Zhang G, Wang J (2014) Photo-Fenton degradation of rhodamine B using Fe_2O_3-Kaolin as heterogeneous catalyst: Characterization, process optimization and mechanism. J Colloid Interface Sci 433:1–8. https://doi.org/10.1016/j.jcis.2014.07.017
8. Fu H, Lin J, Zhang L, Zhu Y (2006) Photocatalytic activities of a novel $ZnWO_4$ catalyst prepared by a hydrothermal process. Appl Catal A: General 306:58–67. https://doi.org/10.1016/j.apcata.2006.03.040
9. Huang G, Zhang C, Zhu Y (2007) $ZnWO_4$ photocatalyst with high activity for degradation of organic contaminants. J Alloy Compd 432(1–2):269–276. https://doi.org/10.1016/j.jallcom.2006.05.109
10. Fu H, Pan C, Zhang L, Zhu Y (2007) Synthesis, characterization and photocatalytic properties of nanosized Bi_2WO_6, $PbWO_4$ and ZnWO4 catalysts. Mater Res Bull 42(4):696–706. https://doi.org/10.1016/j.materresbull.2006.07.017
11. Garadkar KM, Ghule LA, Sapnar KB, Dhole SD (2013) A facile synthesis of $ZnWO_4$ nanoparticles by microwave assisted

technique and its application in photocatalysis. Mater Res Bull 48 (3):1105–1109. https://doi.org/10.1016/j.materresbull.2012.12.002
12. Hosseinpour-Mashkani SM, Maddahfar M, Sobhani-Nasab A (2016) Precipitation synthesis, characterization, morphological control, and photocatalyst application of $ZnWO_4$ nanoparticles. J Electron Mater 45(7):3612–3620. https://doi.org/10.1007/s11664-016-4532-3
13. Sun H, Fan W, Li Y, Cheng X, Li P, Zhao X (2010) Origin of the improved photo-catalytic activity of F-doped $ZnWO_4$: A quantum mechanical study. J Solid State Chem 183(12):3052–3057. https://doi.org/10.1016/j.jssc.2010.10.021
14. Ede SR, Ramadoss A, Nithiyanantham U, Anantharaj S, Kundu S (2015) Bio-molecule assisted aggregation of $ZnWO_4$ nanoparticles (NPs) into chain-like assemblies: material for high performance supercapacitor and as catalyst for benzyl alcohol oxidation. Inorg Chem 54(8):3851–3863. https://doi.org/10.1021/acs.inorgchem.5b00018
15. Yang Y, Zhu J, Shi W, Zhou J, Gong D, Gu S, Wang L, Xu Z, Lu B (2016) 3D nanoporous $ZnWO_4$ nanoparticles with excellent electrochemical performances for supercapacitors. Mater Lett 177:34–38. https://doi.org/10.1016/j.matlet.2016.04.168
16. Guan B, Hu L, Zhang G, Guo D, Fu T, Li J, Duan H, Li C, Li Q (2014) Facile synthesis of $ZnWO_4$ nanowall arrays on Ni foam for high performance supercapacitors. RSC Adv 4(9):4212–4217. https://doi.org/10.1039/C3RA45866K
17. Tang Z, Li X, Yang J, Yu J, Wang J, Tang Z (2014) Mixed potential hydrogen sensor using $ZnWO_4$ sensing electrode. Sens Actuators B Chem 195:520–525. https://doi.org/10.1016/j.snb.2014.01.086
18. You L, Cao Y, Sun YF, Sun P, Zhang T, Du Y, Lu GY (2012) Humidity sensing properties of nanocrystalline $ZnWO_4$ with porous structures. Sens Actuators B Chem 161(1):799–804. https://doi.org/10.1016/j.snb.2011.11.035
19. Zhou Y, Yang L, Zhu M, Dang Y, Peng Z (2016) Hydrothermal method prepared La-doped $ZnWO_4$ nanospheres as electrocatalytic sensing materials for selective and sensitive determination of dopamine and uric acid. J Electrochem Soc 163(14): B737–B743. https://doi.org/10.1149/2.1211614jes
20. Zhan S, Zhou F, Huang N, Liu Y, He Q, Tian Y, Yang Y, Ye F (2017) Synthesis of $ZnWO_4$ electrode with tailored facets: deactivating the microorganisms through photoelectrocatalytic methods. Appl Surf Sci 391:609–616. https://doi.org/10.1016/j.apsusc.2016.06.137. Part B
21. Wang Y, Cai L, Li Y, Tang Y, Xie C (2010) Structural and photoelectrocatalytic characteristic of $ZnO/ZnWO_4/WO_3$ nanocomposites with double heterojunctions. Phys E Low-Dimens Syst Nanostruct 43(1):503–509. https://doi.org/10.1016/j.physe.2010.09.005
22. Jia H, Stark J, Zhou LQ, Ling C, Sekito T, Markin Z (2012) Different catalytic behavior of amorphous and crystalline cobalt tungstate for electrochemical water oxidation. RSC Adv 2 (29):10874–10881. https://doi.org/10.1039/C2RA21993J
23. Ling C, Zhou LQ, Jia H (2014) First-principles study of crystalline $CoWO_4$ as oxygen evolution reaction catalyst. RSC Adv 4 (47):24692–24697. https://doi.org/10.1039/C4RA03893B
24. VKVP Srirapu, Kumar A, Srivastava P, Singh RN, ASK Sinha (2016) Nanosized $CoWO_4$ and $NiWO_4$ as efficient oxygen-evolving electrocatalysts. Electrochim Acta 209:75–84. https://doi.org/10.1016/j.electacta.2016.05.042
25. Chen S, Yang G, Jia Y, Zheng H (2016) Facile synthesis of $CoWO_4$ nanosheet arrays grown on nickel foam substrates for asymmetric supercapacitors. ChemElectroChem 3(9):1490–1496. https://doi.org/10.1002/celc.201600316
26. Saranya M, Ramachandran R, Wang F (2016) Graphene-zinc oxide (G-ZnO) nanocomposite for electrochemical supercapacitor applications. J Sci: Adv Mater Devices 1(4):454–460. https://doi.org/10.1016/j.jsamd.2016.10.001
27. Lu T, Zhang Y, Li H, Pan L, Li Y, Sun Z (2010) Electrochemical behaviors of graphene–ZnO and graphene–SnO_2 composite films for supercapacitors. Electrochim Acta 55(13):4170–4173. https://doi.org/10.1016/j.electacta.2010.02.095
28. Kumar RD, Andou Y, Karuppuchamy S (2016) Synthesis and characterization of nanostructured Ni-WO_3 and $NiWO_4$ for supercapacitor applications. J Alloy Compd 654:349–356. https://doi.org/10.1016/j.jallcom.2015.09.106
29. Dhilip Kumar R, Andou Y, Sathish M, Karuppuchamy S (2016) Synthesis of nanostructured Cu-WO_3 and $CuWO_4$ for supercapacitor applications. J Mater Sci Mater Electron 27 (3):2926–2932. https://doi.org/10.1007/s10854-015-4111-z
30. AlShehri SM, Ahmed J, Ahamad T, Almaswari BM, Khan A (2017) Efficient photodegradation of methylthioninium chloride dye in aqueous using barium tungstate nanoparticles. J Nanopart Res 19(8):289. https://doi.org/10.1007/s11051-017-3970-z
31. AlShehri SM, Ahmed J, Alzahrani AM, Ahamad T (2017) Synthesis, characterization, and enhanced photocatalytic properties of $NiWO_4$ nanobricks. New J Chem 41(16):8178–8186. https://doi.org/10.1039/C7NJ02085F
32. AlShehri SM, Ahmed J, Ahamad T, Arunachalam P, Ahmad T, Khan A (2017) Bifunctional electro-catalytic performances of $CoWO_4$ nanocubes for water redox reactions (OER/ORR). RSC Adv 7:45615–45623
33. Ahmed J, Ahamad T, AlShehri SM (2017) Iron–Nickel Nanoparticles as Bifunctional Catalysts in Water Electrolysis. ChemElectroChem 4(5):1222–1226. https://doi.org/10.1002/celc.201600754
34. Alshehri SM, Ahmed J, Alhabarah AN, Ahamad T, Ahmad T (2017). Nitrogen-doped cobalt ferrite/carbon nanocomposites for supercapacitor applications. ChemElectroChem. https://doi.org/10.1002/celc.201700602
35. Kim M-J, Huh Y-D (2010) Ligand-assisted hydrothermal synthesis of $ZnWO_4$ rods and their photocatalytic activities. Mater Res Bull 45(12):1921–1924. https://doi.org/10.1016/j.materresbull.2010.08.018
36. Hojamberdiev M, Zhu G, Xu Y (2010) Template-free synthesis of $ZnWO_4$ powders via hydrothermal process in a wide pH range. Mater Res Bull 45(12):1934–1940. https://doi.org/10.1016/j.materresbull.2010.08.015
37. He G, Fan H, Ma L, Wang K, Ding D, Liu C, Wang Z (2016) Synthesis, characterization and optical properties of nanostructured $ZnWO_4$. Mater Sci Semicond Process 41:404–410. https://doi.org/10.1016/j.mssp.2015.09.025
38. Ungelenk J, Speldrich M, Dronskowski R, Feldmann C (2014) Polyol-mediated low-temperature synthesis of crystalline tungstate nanoparticles MWO_4 (M = Mn, Fe, Co, Ni, Cu, Zn). Solid State Sci 31:62–69. https://doi.org/10.1016/j.solidstatesciences.2014.02.020
39. Mancheva M, Iordanova R, Dimitriev Y (2011) Mechanochemical synthesis of nanocrystalline $ZnWO_4$ at room temperature. J Alloy Compd 509(1):15–20. https://doi.org/10.1016/j.jallcom.2010.08.033
40. Amouzegar Z, Naghizadeh R, Rezaie HR, Ghahari M, Aminzare M (2015) Cubic $ZnWO_4$ nano-photocatalysts synthesized by the microwave-assisted precipitation technique. Ceram Int 41:1743–1747. https://doi.org/10.1016/j.ceramint.2014.09.119. (1, Part B)
41. Amouzegar Z, Naghizadeh R, Rezaie HR, Ghahari M, Aminzare M (2015) Microwave engineering of $ZnWO_4$ nanostructures: Towards morphologically favorable structures for photocatalytic activity. Ceram Int 41(7):8352–8359. https://doi.org/10.1016/j.ceramint.2015.03.020

42. Bi J, Wu L, Li Z, Ding Z, Wang X, Fu X (2009) A facile microwave solvothermal process to synthesize $ZnWO_4$ nanoparticles. J Alloy Compd 480(2):684–688. https://doi.org/10.1016/j.jallcom.2009.02.029
43. Huang Y, Gao Y, Zhang Q, Cao J-j, Huang R-j, Ho W, Lee SC (2016) Hierarchical porous $ZnWO_4$ microspheres synthesized by ultrasonic spray pyrolysis: Characterization, mechanistic and photocatalytic NOx removal studies. Appl A General 515:170–178. https://doi.org/10.1016/j.apcata.2016.02.007
44. Yan B, Lei F (2010) Molten salt synthesis, characterization and luminescence of $ZnWO_4$:Eu_3+ nanophosphors. J Alloy Compd 507(2):460–464. https://doi.org/10.1016/j.jallcom.2010.07.203
45. Kramer CM, Wilson CJ (1980) The phase diagram of $NaNO_3$—KNO_3. Thermochim Acta 42(3):253–264. https://doi.org/10.1016/0040-6031(80)85085-4
46. Liu Y, Wang H, Chen G, Zhou YD, Gu BY, Hu BQ (1988) Analysis of Raman spectra of $ZnWO_4$ single crystals. J Appl Phys 64(9):4651–4653. https://doi.org/10.1063/1.341245
47. Zhou R, Zheng Y, Jaroniec M, Qiao S-Z (2016) Determination of the electron transfer number for the oxygen reduction reaction: from theory to experiment. ACS Catal 6(7):4720–4728. https://doi.org/10.1021/acscatal.6b01581
48. Wu Z, Li W, Xia Y, Webley P, Zhao D (2012) Ordered mesoporous graphitized pyrolytic carbon materials: synthesis, graphitization, and electrochemical properties. J Mater Chem 22 (18):8835–8845. https://doi.org/10.1039/C2JM30192J
49. Reddy ALM, Gowda SR, Shaijumon MM, Ajayan PM (2012) Hybrid nanostructures for energy storage applications. Adv Mater 24(37):5045–5064. https://doi.org/10.1002/adma.201104502
50. Brun N, Prabaharan SRS, Surcin C, Morcrette M, Deleuze H, Birot M, Babot O, Achard MF, Backov R (2012) Design of hierarchical porous carbonaceous foams from a dual-template approach and their use as electrochemical capacitor and Li ion battery negative electrodes. J Phys Chem C 116(1):1408–1421. https://doi.org/10.1021/jp206487w
51. Srivastava M, Singh J, Kuila T, Layek RK, Kim NH, Lee JH (2015) Recent advances in graphene and its metal-oxide hybrid nanostructures for lithium-ion batteries. Nanoscale 7 (11):4820–4868. https://doi.org/10.1039/c4nr07068b
52. Tauc J (1968) Optical properties and electronic structure of amorphous Ge and Si. Mater Res Bull 3(1):37–46. https://doi.org/10.1016/0025-5408(68)90023-8
53. Zhang C, Zhang H, Zhang K, Li X, Leng Q, Hu C (2014) Photocatalytic activity of $ZnWO_4$: band structure, morphology and surface modification. ACS Appl Mater Interfaces 6 (16):14423–14432. https://doi.org/10.1021/am503696b
54. Montini T, Gombac V, Hameed A, Felisari L, Adami G, Fornasiero P (2010) Synthesis, characterization and photocatalytic performance of transition metal tungstates. Chem Phys Lett 498 (1–3):113–119. https://doi.org/10.1016/j.cplett.2010.08.026
55. Ahmed B, Kumar S, Ojha AK, Donfack P, Materny A (2017) Facile and controlled synthesis of aligned WO_3 nanorods and nanosheets as an efficient photocatalyst material. Spectrochim Acta Part A Mol Biomol Spectrosc 175:250–261. https://doi.org/10.1016/j.saa.2016.11.044